3D Flame Reconstruction Using Single Camera and Fibers

Kuanliang Wang[1,2], Fei Li[1,*], and Xilong Yu[1,2]
1State Key Laboratory of High Temperature Gas Dynamics, Institute of Mechanics, CAS, Beijing 100190, China

2 School of Engineering Science, University of Chinese Academy of Sciences, Beijing 100049, China

1 Introduction

Chemiluminescence measurement of combustion is an important pointer for heat release rate [1,2], equivalence ratio [2], excited species concentrations [3], using the emitted photons of combustion reaction without lasers that can be taken in harsh condition. Based on the tomography method, we can achieve the temporal resolved three-dimensional (3D) measurements. In recent years, CTC techniques have been widely studied due to the great improvements of capabilities of optical sensing and computing technologies. These techniques use multiple 2D projections from various views of the target flame, combined with reconstruction algorithms to obtain high resolution 3D measurements. The multi-directional 2D projections can be realized by lens and CCD cameras [4-8] or by fiber-based endoscopes (FBEs) with multi-CCD [9,10]. Till now, most 3D-CTC works based on the parallel projection model [4-7], considering the singles integral measurements are parallel from the reconstruction region, which may be incorrect under short object distance. In order to obtain a more accurate reconstruction the simulation of imaging process is vital. There are various studies related to the imaging process in different optical system. Walsh [11] proposed ray-tracing simulation to study the effect of light-collection geometry on reconstruction errors in Abel inversions. Xuesong Li [12] and MinWook Kang [13] used the point spread function(PSF) as the weighting factor of the signals contributed from voxels to pixels. In their works, the PSF was computed using a Monte Carlo (MC) method by simulating and tracing the generated photons in random directions. Jia Wang [8] proposed camera calibration method to determine the spatial locations and intrinsic parameters of the cameras. They have taken the size of blurry circle because of out-of-focus effects into account, using the separation of the two circle centers (blurry circle and pixel) to weight the contributions of each voxel to the pixels.

In this paper, we proposed modified projection models based on the blurring function and lens imaging theory. The blurring function here we used to describe the intensity distribution of blurry circle was obtained by fluorescent beads. Only one CCD was utilized to build 3D-CTC system combined with customized fiber-based endoscopes (FBEs) to improve adaptability, which makes this technique more

Correspondence to: lifei@imech.ac.cn

economic and simple. Validate experiments were made using 10 small CH4 diffusion flame arranging in a ring structure. Projections captured by the optical system were used as inputs of projection model integrated with Algebraic Reconstruction Technique (ART) algorithm to compute the reconstruction of target flame. Results are compared with the blurring function taken or not into account. A projections deconvolution pretreatment method was also proposed to solve the blurring effect of 3D-CTC system.

2.mathematical formulation

The mathematical formation of the CTC problem can be illustrated by Fig.1. If we use F(x,y,z) to denote the 3D distribution of the chemiluminescence signals emitted from object domain, the projection measured (Ip) from a viewing angle (q) can then be defined in Eq.1. The viewing angles can be specified by r (distance), θ (azimuth angle), and ϕ (inclination angle), and W is Weight matrix represents the relationship between pixel and the corresponding position of objective region. Projection of pixels determined by these angles and the intrinsic parameters of the camera.

$$I_{pq} = F(x, y, z) \cdot W(x, y, z; p, q) \tag{1}$$

To solve the tomgraphic problem various iterative algorithms were created, and the most widely used one is Algebraic Reconstruction Technique(ART). It was firstly developed by Gordon to solve the 3D reconstruction problem from projection of electron microscopy and radiology. In our reconstruction work, an additive version of ART was utilized, which has also been adopted by Flord[6,7], as described in Eq. (2).

$$F^{(k+1)} = F^{(k)} + \lambda \cdot \boldsymbol{W} \frac{I_{pq} - \boldsymbol{W} \cdot F^{(k)}}{\boldsymbol{W} \cdot \boldsymbol{W}} \tag{2}$$

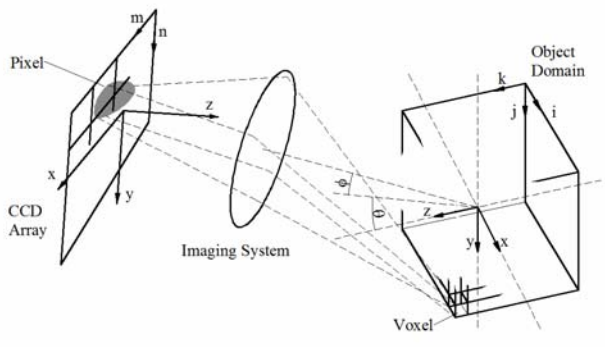

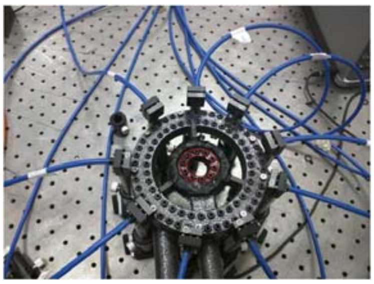

Fig.1 (a) Mathematical formulation of 3D-CTC (b) 3D-CTC system with 9 customized FBEs

3. Experiments setups

To determine the imaged centre position on the pixel of random spatial point from the object domain, we utilized the calibration method proposed by Jia Wang[8]. In our calibration, luminescent spot produced by a He-Ne laser serves as space point source, which can move three dimensional. And the imaging position was conformed via centre point extracting algorithm.

In our 3D-CTC system, only one CCD was utilized combined with customized FBEs, which has 9 inputs and 1 outputs. Each inputs is an assembling of 13,000 fibers, so the output end transits 117,000 image elements to CCD. The pixel size of CCD (IMI 147FT) is 6.45um*6.45um. These 9 lens of input end array scattered around the flame, as shown in Fig1(b).

The validation experiment was conducted on a bunner with 10 holes on the jet nozzle that can generate 10 small CH_4 diffusion flames arranging in a ring structure, is shown in Fig.2. The inner and outer diameter of the flames were 25.18mm and 37.74mm, and the size of each flame was slightly bigger than the diameter of the single hole, which was about 5.2 mm. projections are taken simultaneously by one CCD (IMI 147FT: pixel size 6.45um×6.45um) via the customized FBEs. The case of projections for the reconstruction work is shown in Fig.3

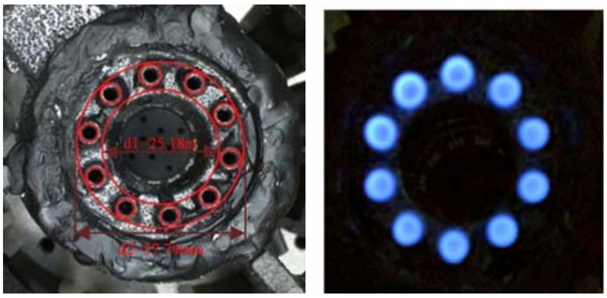

Fig.2 jet nozzle and CH_4 diffusion flames

Fig.3 Simultaneous projections of the CH_4 diffusion flames

4. Blurring function calibration

Considering the imaging of CCD is based on the conversion of incoming photons into electron charges, except the intersection area of pixel and blurred circle from object point, the intensity distribution of blurry circle can also be an important factor. In order to understand the actual distribution of blurred circle from the point light source, a fluorescent bead about hundred-micron magnitude was used to calibrate the blurring function on the pixels. We placed the bead at several random positions of the object domain, and the blurry circle measured of certain position is show in Fig4 (a). For simplification, we assume that the intensity distribution is central symmetry, and find that the Gaussian function can fit the intensity in radial direction appropriately. The fitting results for these positions are shown in Fig4 (b).

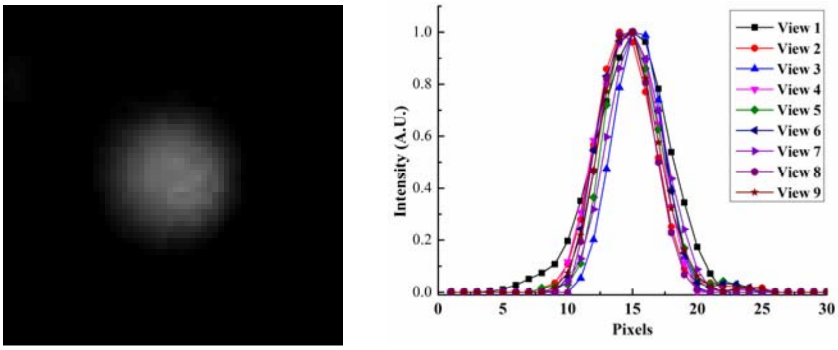

(a) blurry circle from the point light source (b) Gaussian fittings of intensity distribution

Fig.4 Imaging of one point light source

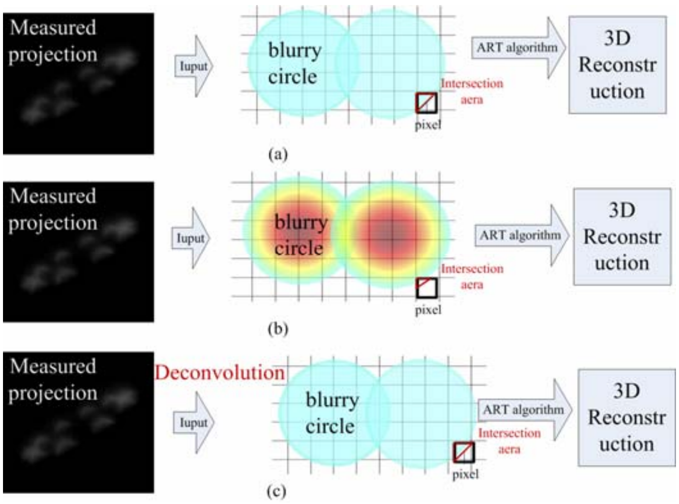

Fig.5 projections processing models

Table 1 Procedure setting

projections processing models	Voxel number (x*y*z)	Voxel size [mm]	Iterations	Running time [sec]
(a)	120*120*30	0.375*0.375*0.67	2000	8175
(b)	120*120*30	0.375*0.375*0.67	2000	141532
(c)	120*120*30	0.375*0.375*0.67	2000	8205

Three projections processing models are proposed as shown in Fig.5.First one is shown in Fig5(a):measured projections are used as input data, and the weight factors of the voxel to the pixels are determined by intersection areas of the blurry circle with the pixels; (b) Measured projections are used as input data, and the weight factors of the voxel to the pixels are determined by intersection areas multiply the intensity fitted by Gaussian function corresponded with the separation between pixels and the blurred circle center; (c) Deconvolution artifacts of measured projections are used as input data, and the weight factors of the voxel to the pixels are determined by intersection areas of the blurry circle with the pixels. To simplify the calculation, we approximate the intersection area which can not covered completely by blurred circle as polygons. Analyses are made by comparing with the resulting data of reconstructions. Procedure setting is shown in Table.1. For the same procedure setting the running time for model (b) is 141532 seconds, which 17 times more than model (a) and (c).

5. Results and analysis

Fig6 shows the vertical view of reconstructed flame using the projections in Fig3. As shown in Figure 6(a),(b),(c), We can firmly see 10 small flames arranging in a ring structure. The diameter of inner circle is about 70 voxels, and the outer circle is about 110 voxels, which well match the flame shown in Fig2. There are slight visual differences among (a), (b) and (c). Fig.7 illustrates the visual observations by examining the intensity distribution between the red circles on Fig.6. Analyzing the bottom value between number 5 and 6 flames (number 10 and 1 flames) that the reconstructed intensity value based on model (b) is smaller than model (c), while model (a) is largest. It indicate that model (b) is closer to the actual value since these small flames is basically isolated to each other.

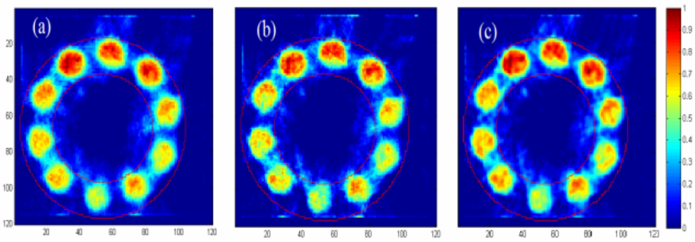

Fig.6 Vertical view of reconstructed flame

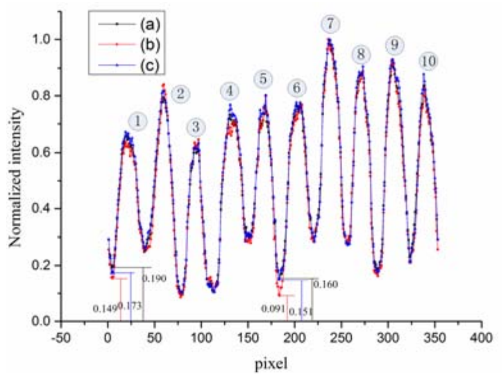

Fig.7 Normalized intensity between the red circles

6. Summary and conclusion

In this study, overall approaches for 3D-CTC were carried out to investigate effect of blurring function. The experiment system was based on customized fibers and one CCD camera. Blurring function was calibrated and three modified projections models were proposed. Reconstruction results are compared that illustrate a better resolution for the consideration of blurring effect. The projection backward processing method that utilizing deconvolution to replace the forward adding of blurring function can also achieved better reconstruction works than the method ignore blurring effect.

Acknowledgments

This work was sponsored by the National Natural Science Foundation of China (Grant nos.11372329).

References

[1] Zhang T, Guo Q, Song X, Zhou Z, Yu G. (2013). The Chemiluminescence and Structure Properties of Normal/Inverse Diffusion Flames. J. Spectro. 1:133.

[2] Docquier N, Lacas F, Candel S. (2002) Closed-loop equivalence ratio control of premixed combustors using spectrally resolved chemiluminescence measurements. Proc. Combust. Inst.1: 139.

[3] Smith GP, Luque J, Park C, Jeffries JB, Crosley DR.(2002). Low pressure flame determinations of rate constants for OH (A) and CH (A) chemiluminescence. Combust Flame. 1: 59.

[6] Wan X, Xiong W, Zhang Z, Zhang F.(2009) An online emission spectral tomography system with digital signal processor. Opt express. 17: 5279.

[7] Gao Y, Yu Q, Jiang W, Wang X. (2010) Reconstruction of three-dimensional arc-plasma temperature fields by orthographic and double-wave spectral tomography. Opt Laser Technol.42: 61.

[8] Floyd J, Geipel P, Kempf A M.(2011) Computed tomography of chemiluminescence (CTC): instantaneous 3D measurements and phantom studies of a turbulent opposed jet flame. Combust Flame.158: 376.

[9] Floyd J, Kempf A M.(2011) Computed tomography of chemiluminescence (CTC): high resolution and instantaneous 3-D measurements of a matrix burner. Proc. Combust. Inst. 33: 751.

[10] Wang J, Song Y, Li Z, Kempf A, He A.(2015) Multi-directional 3D flame chemiluminescence tomography based on lens imaging. Opt express.40: 1231.

[11] Kang M W, Wu Y, Ma L.(2014) Fiber-based endoscopes for 3D combustion measurements: view registration and spatial resolution. Combust Flame. 2014, 161: 3063.

[12] Ma L, Lei Q, Wu Y, Ombrello TM, Carter CD.(2015) 3D measurements of ignition processes at 20 kHz in a supersonic combustor. Appl Phys B-Lasers O. 119: 313.

[13] Walsh K T, Fielding J, Long M B.(2000) Effect of light-collection geometry on reconstruction errors in Abel inversions. Opt Lett, 25: 457.

[14] Li X, Ma L. (2015) Capabilities and limitations of 3D flame measurements based on computed tomography of chemiluminescence. Combust Flame. 162: 642.

[15] Kang M W, Li X, Ma L.(2015) Three-dimensional flame measurements using fiber-based endoscopes. Proc. Combust. Inst. 35: 3821.